

Effect of target geometry on compression of ions into a shell in a laser plasma expanding into vacuum

V. V. Maksimov, A. M. Orishich, A. G. Ponomarenko, and V. N. Snytnikov

Institute of Theoretical and Applied Mechanics, Siberian Branch, Academy of Sciences of the USSR

(Submitted 5 October 1988; resubmitted 1 March 1989)

Zh. Eksp. Teor. Fiz. **96**, 1253–1261 (October 1989)

A new regime in the expansion of a laser plasma into vacuum has been studied. In this regime, the number of fast ions increases sharply, and a thin shell containing up to half the total energy and a quarter of the total number of particles forms at the vacuum boundary of the plasma. The motion of this shell is stable. This transformation of the ion distribution function is achieved by applying microsecond CO₂ laser pulses to cylindrical and spherical targets. A model for the compression of the ions of the plasma corona into the shell is proposed. This model is based on the time variation of the absorption of radiant energy, the change in the flux of particles from the target, and the collective interaction of the ions in the course of the expansion. The target geometry plays an important role in the appearance of this shell structure in the plasma corona.

1. INTRODUCTION

Most of the research on the interaction of laser light with matter is aimed at laser fusion or the development of new fields of technology.^{1,2} The plasmas produced as a result of this interaction have found applications in the laboratory modeling of processes of interest in space physics.³ This research requires an understanding of just how the plasma expands into vacuum. A general result of the numerous experimental and theoretical studies of the expansion of a plasma is the conclusion that the density decays essentially monotonically, usually exponentially, with distance from the source.⁴ Exceptional cases are local features near the critical density and the vacuum ion front, with a length scale on the order of the Debye length.^{1,4} Our experiments,⁵ however, have revealed a regime in which the laser plasma expands in the form of a thin, stable spherical shell which contains up to 50% of the total energy and up to 25% of the total number of particles. The existence of this shell has been linked with the time variation of the plasma outflow conditions near the source.⁶ In the present paper we are reporting a detailed study, including experiments and numerical simulations, of the entire ion compression process, starting at the target, and also of the role played by the target geometry in the formation of the shell during the expansion of the laser plasma into vacuum.

2. EXPERIMENTAL RESULTS

1. The experiments were carried out on the KI-1 facility⁵, which was constructed for laboratory modeling of time-varying astrophysical phenomena. Laser plasmas are used in this research, e.g., in experiments on the mechanisms for the collisionless slowing of the envelopes of supernovae by the surrounding medium.⁷ The facility includes a vacuum chamber 1.2 m in diameter and 5 m long with a residual pressure of 10⁻⁶ torr and a source of laser light, with a pulse length which is adjustable over the range 0.1–3.0 μ s, with a wavelength $\lambda = 10.6 \mu\text{m}$, and with an energy $\sim 1 \text{ kJ}$.

In the experiments we used targets of three types: a spherical target 1–3 mm in diameter, a cylindrical target, which was a filament 0.3 mm in diameter, and a plane target, which was a plate 5 mm thick. All the targets were made of polymerized caproactam, (C₆H₁₁ON)_n. The spherical tar-

get was suspended on a thin metal filament 0.1 mm in diameter. The laser beam was split up into two identical beams, which were focused in opposite radial directions onto a tablet at the center of the chamber, and at its axis. The plane target was put in the same place but was illuminated from one side, at an angle $\theta = 15^\circ$ from the normal to the surface. The cross-sectional area of the beam in the target region was $\approx 4 \times 4 = 16 \text{ mm}^2$. In these experiments we used a bell-shaped pulse with an adjustable length at half-maximum (from 0.05 to 0.5 μs). The average power density on the target varied from shot to shot in the range $2 \cdot 10^8$ – $2 \cdot 10^9 \text{ W/cm}^2$.

The plasma density n_e and the ion flux density at distances $r \approx 20$ –60 cm and at $n_e < 10^{14} \text{ cm}^{-3}$ were measured by double electrostatic probes⁸ and ion collectors.⁹ A large number (8–10) of special leads and also some movable probes made it possible to carry out measurements simultaneously at various angles (θ and φ) and at various distances from the target. The shape of the cloud was also monitored photographically with the help of an image converter. The charge and mass composition of the plasma was determined by a time-of-flight analyzer like that of Ref. 9.

To measure the plasma density in the range $n_e \approx 3 \cdot 10^{18}$ – 10^{14} cm^{-3} we used the following interferometers: (a) a Mach-Zehnder interferometer, with $\lambda = 0.694 \mu\text{m}$, with visualization of a field of $50 \times 50 \text{ mm}^2$ and with a sensitivity of ~ 0.1 of a fringe. The measurement range here was $n_e \sim 10^{17}$ – $3 \cdot 10^{18} \text{ cm}^{-3}$. (b) Mach-Zehnder interferometers with photoelectric detection, with $\lambda = 0.633 \mu\text{m}$ and $\lambda = 10.6 \mu\text{m}$, with a time resolution $\lesssim 5 \text{ ns}$, and with a spatial resolution $\sim 1 \text{ mm}$. The measurement error here was $\pm 0.5 \cdot 10^{-3}$ of a fringe. These interferometers were used to study the plasma dynamics in the range $n_e \approx 10^{17}$ – 10^{14} cm^{-3} ($r = 1$ –9 cm, $\lambda = 0.63 \mu\text{m}$) and $n_e \approx 10^{13}$ – 10^{15} cm^{-3} ($r \approx 10$ –18 cm, $\lambda = 10.6 \mu\text{m}$). The measurements were carried out at distances $r = 1, 2, 4, 6, 12$, and 17 cm. The radial profile $n_e(r)$ was calculated through numerical integration of the inverted Abel equation.

The total number of particles N and the energy E were determined by the method described in detail in Ref. 10 and also by integration of the distribution $n_e(r)$.

2. The measurements showed that the distribution of

the number of particles in the cloud which are moving into a unit solid angle,

$$\frac{dN}{d\Omega} = R^2 \int j_r dt,$$

is determined by the target geometry. For a plane target, for example, we observed the familiar distribution $dN/d\Omega \sim \cos^m \theta$, where $m = 2-3$ and the angle θ is measured from the normal to the surface. In the case in which the length of a cylindrical target exceeded the beam diameter while the target was being illuminated from two sides, we found a similar distribution in the plane of the axis of the filament: $dN/d\Omega \propto j_r \propto \sin^m \alpha$, where α is the angle from the axis. In the plane perpendicular to the filament and containing the laser beams, we observed a flux which was axisymmetric with respect to the axis of the target. The differences in the parameter values measured at various angles φ was at most $\pm 15\%$ in terms of the number of particles or $\pm 5\%$ in terms of the average velocity.

When we used a circular target we were able to produce a spherical cloud. This symmetry was retained up to a tablet diameter of 3 mm, which is comparable to the size of the beam, ≈ 4 mm. In this case the flux contained $N \approx 3 \cdot 10^{18}$ particles with a total energy $E \approx 125$ J.

Under our experimental conditions, at the relatively low power $q \sim 10^9$ W/cm², the plasma flux distribution in the selected spatial plane was thus determined by the geometry of the intersection of the target with this plane. In particular, during the illumination of a filament the flux exhibited properties of both a sphere (axial symmetry) and a plane (the plasma distribution along the filament).

3. The measurements showed that at a given power level of the incident light the dynamics of the laser plasma and the density distribution $n_e(r, t)$ which is produced depend strongly on the length of the light pulse and the target geometry.

Near the surface the nature of the flow and the behavior of the density are determined by the target parameters. Figure 1 shows some typical profiles $n_e(r)$ in the interval $3 \cdot 10^{18}$ – 10^{15} cm⁻³ for $\nu = 0$ (a plane target) and $\nu = 1$ (a cylindrical target). These profiles are along the axis which runs perpendicular to the surface and passes through the center of the laser beam. In the case of the plane target, the plasma is seen to build up to a level $n_e(r) = \text{const}$ over a scale $r \lesssim \phi$, in complete accordance with a one-dimensional flow regime. At large distances $r > \phi$ the flux ceases to be one-dimension-

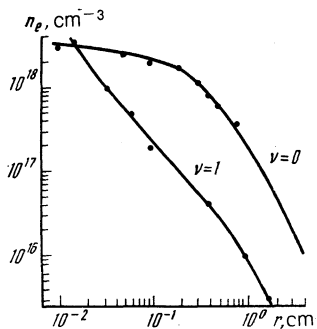


FIG. 1. Profiles of the electron density near the surface of a plane target ($\nu = 0$) and a cylindrical target ($\nu = 1$) exposed to a laser pulse with a length $\tau = 0.5 \mu\text{s}$ at half-maximum.

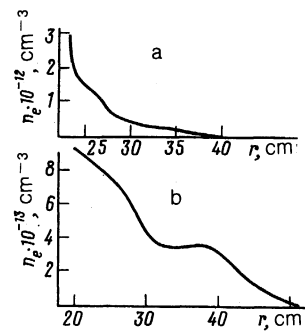


FIG. 2. Profiles of the electron density of the laser plasma near a plane target during exposure to (a) a short light pulse, with $\tau = 0.1 \mu\text{s}$, and (b) a long one, with $\tau = 0.5 \mu\text{s}$. a—The time, t , at the beginning of the pulse is 3 μs ; b—2.7 μs .

al, as transverse expansion begins to play an important role. The density decreases in accordance with $n_e(r) \propto r^{-1.8}$. Near a thin filament ($\nu = 1$) we observe a monotonic decay $n_e(r) \propto r^{-1.3}$ (Fig. 1).

Figures 2 and 3 show the plasma density profiles in the range $n_e \approx 10^{15}$ – 10^{12} cm⁻³ at distances 1–40 cm from the target. In the case of a short pulse, with $\tau \lesssim 0.1 \mu\text{s}$, which is comparable to the hydrodynamic acceleration time $\tau_s \sim (1-10)\phi/c_s$, where ϕ is the size of the illuminated part of the target, and c_s is the sound velocity, the profile $n_e(r)$ decreases monotonically with distance for any target configuration (Fig. 2a).

An increase in τ_s to $(10^2-10^3) \phi/c_s$ for spherical or cylindrical pellets resulted in a fundamental change in the dynamics of the laser plasma. As Fig. 3a shows, a plateau begins to form on the $n_e(r)$ profile as early as $t = 0.41 \mu\text{s}$. This actually means that there is a relative increase in the number of fast particles which are reaching the front of the cloud. A further increase in the relative number of such ions after the end of the light pulse creates a density peak (Fig.

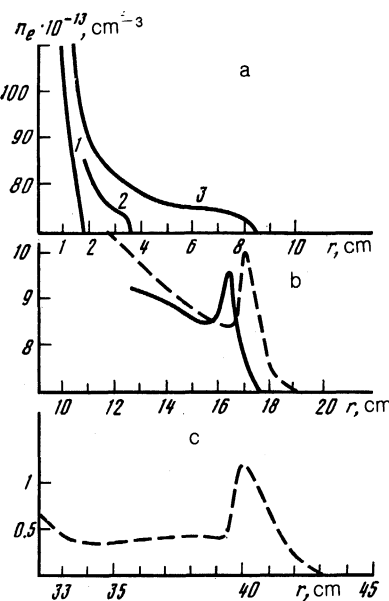


FIG. 3. Plasma density profiles at various times. a: 1— $t = 0.2$; 2— 0.41 ; 3— $0.9 \mu\text{s}$. b: $t = 1.5 \mu\text{s}$. c: $t = 2.7 \mu\text{s}$. Here a cylindrical target was exposed to a laser pulse with a length $\tau = 0.5 \mu\text{s}$. Solid lines) data obtained with the interferometers; dashed lines) data obtained with the probes.

3b). In the case of the circular pellet, this process leads to the creation of a spherical plasma shell at the front of the cloud, containing up to 40% of the total number of particles in the cloud. The shell contains both light hydrogen ions and ions of carbon, with a maximum charge $Z = 4$ for this plasma. In the case of the cylindrical target, the shell, marked by the arrows in Fig. 4, is axisymmetric with respect to an axis, propagates in the angular interval $\alpha = 60 \pm 120^\circ$, and contains up to $\sim 25\%$ of the particles. This photograph was taken with the help of an image converter⁵ with a delay $\tau = 3.6 \mu\text{s}$; the shell radius is $\sim 36 \text{ cm}$.

Analysis of profiles of the type in Fig. 3 shows that the velocity of the front of the cloud increases throughout the light pulse, i.e., essentially over the time required for the formation of the shell ($\sim 1 \mu\text{s}$) at a scale $r \sim V_\tau \sim 10-15 \text{ cm}$ (V is the average velocity of the envelope). At large distance ($r > V_\tau$) the motion of the shell is inertial, at a constant velocity. The shell thickness increases from $\Delta r = 1-1.5 \text{ cm}$ at $r = 20 \text{ cm}$ to $\Delta r = 4 \text{ cm}$ at $r = 60 \text{ cm}$, while the density falls off in accordance with $n \sim r^{-3}$. The number of particles in the shell remains constant within the measurement error ($\pm 20\%$) in this stage of the process.

We studied the formation of the shell at the front of the cloud. Previous experiments⁵ had shown that as the light pulse length is increased to $\tau \approx 3 \mu\text{s}$ there may be an expansion of plasma in the form of two or even three shells. These shells are apparently produced at different times, according to an analysis of their $R-t$ diagrams.

To conclude our discussion of the experimental data, we consider the effect of recombination on the formation of the observed structure of the cloud. During the application of short-wave light ($\lambda \lesssim 1 \mu\text{m}$, $n_{\text{cr}} \gtrsim 10^{21} \text{ cm}^{-3}$) to a target, we know^{11,12} that the ion composition of the plasma is determined by recombination and is characterized by a sharp decrease in the number of ions with increasing ion charge. An increase in the wavelength to $10.6 \mu\text{m}$ and a reduction of the critical plasma density to $n_{\text{cr}} \approx 10^{19} \text{ cm}^{-3}$ substantially change the charge composition of the plasma, in the direction of an increase in the average charge of the particles.¹³ According to our measurements, during quasisteady heating for $\sim 1 \mu\text{s}$, i.e., during the expansion of the plasma to $r \approx 10-15 \text{ cm}$, the cloud consists of protons and multiply charged carbon ions (55% H^+ , 30% C^{4+} , and 15% C^{3+} ; Ref. 14).

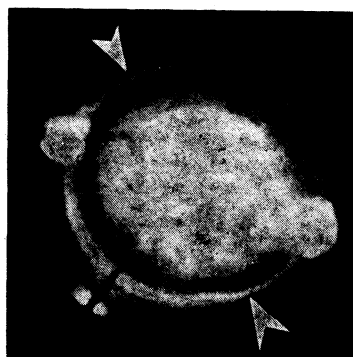


FIG. 4. Photograph of an expanding laser plasma. The exposure time is 50 ns. The bright central region is the slow part of the plasma. The two symmetric spots at the radius of the shell are the mirrors which focus the light onto the target.

The apparent interpretation is a decrease in the effectiveness of recombination, with the ionization rate and the velocity of the gas-dynamic expansion playing a dominant role.¹⁵

3. NUMERICAL MODEL OF THE DYNAMICS OF A LASER PLASMA DURING TIME-VARYING PLASMA OUTFLOW

The set of experimental results suggests the following interpretation. As the pulse length is increased, the time variation of the plasma production near the target begins to have a strong effect on the dynamics of the plasma corona. This time variation results from both the finite width of the front of the light pulse, which is greater than the gas-dynamics length scales, and the instability of the process by which the plasma is produced during the application of the light to the target.¹⁶ The result may be the formation of a plasma cloud with a continuously varying velocity or of several successive plasmoids, which expand away from the target at different velocities. The interaction of these plasmoids occurs at distances $r \gg R_0$ (R_0 is the target radius), in the stage of the inertial gas-dynamics motion, i.e., in a manner independent of M/Z . This interaction leads to restructuring of the plasma cloud.

The numerical simulation of the dynamics of the corona expansion was carried out for moderate power densities of the light, $q \lesssim 10^{10} \text{ W/cm}^2$. These values correspond to ion and electron temperatures $T_{e,i} \lesssim 30 \text{ eV}$ near the point with the critical density $n_{\text{cr}} \approx 10^{19} \text{ cm}^{-3}$ (Ref. 11). At these parameter values the mean free path is $l \sim 6 \cdot 10^{-4} \text{ cm}$ and the condition $l/R_0 \ll 1$ holds so we can use the single-velocity hydrodynamic equations near the target:

$$\begin{aligned} \frac{\partial n}{\partial t} + \nabla(n\mathbf{u}) &= 0, \\ \rho \left[\frac{\partial \mathbf{u}}{\partial t} + (\mathbf{u}\nabla)\mathbf{u} \right] &= -\nabla(p_i + p_e) + [\mathbf{jB}], \\ n \frac{1}{\gamma - 1} \left[\frac{\partial T_i}{\partial t} + (\mathbf{u}\Delta)T_i \right] + p_i \nabla \mathbf{u} &= -\nabla \mathbf{q}_i + Q_i, \\ n \frac{1}{\gamma - 1} \left[\frac{\partial T_e}{\partial t} + (\mathbf{u}\Delta)T_e \right] + p_e \nabla \mathbf{u} &= -\nabla \mathbf{q}_e + Q_e. \end{aligned}$$

If we assume an adiabatic expansion of the corona with $\gamma = 5/3$, then the mean free path $l \sim T^2/n \sim n^{2(\gamma-1)}$ falls off with distance from the target, and the condition for a collisional regime is satisfied better. Estimating the length scale of the thermal conductivity, $(D_t t)^{1/2} \sim (lv_{te} t)^{1/2} \sim 0.4 \text{ cm}$ with $t \approx 1 \mu\text{s}$, and examining the formation of the shell at distances $r \approx 8-15 \text{ cm}$, we ignore (in a first approximation) the heat fluxes, the deviation of the electron temperature from the ion temperature, and the magnetic fields during an expansion which is not spherically symmetric. Working from the experimental data, which show a decrease $n_e \sim r^{-3}$ in the electron density after the end of the laser pulse, i.e., working from the position that the additional heating due to possible three-particle recombination does not affect the expansion and also the fact that the shell and the cloud consist primarily of C^{4+} ions, with an ionization potential $U_4 = 64 \text{ eV}$, and hydrogen ions H^+ , we eliminated recombination from the original equations.

As a result of the simplifications, the one-dimensional hydrodynamic model for the formation of the shell with a single ion species (hydrogen) takes the form

$$\begin{aligned} \frac{\partial n}{\partial t} + \frac{1}{r^v} \frac{\partial}{\partial r} (r^v n u) &= 0, \\ \frac{\partial (n u)}{\partial t} + \frac{1}{r^v} \frac{\partial}{\partial r} (r^v n u^2) &= -\frac{\partial p}{\partial r}, \quad p = n T, \\ \frac{\partial e}{\partial t} + \frac{1}{r^v} \frac{\partial}{\partial r} [u r^v (e + p)] &= 0, \quad e = n T (\gamma - 1)^{-1} + n u^2 / 2, \end{aligned} \quad (1)$$

where $v = 0, 1, 2$ is a geometric factor which distinguishes the planar, cylindrical, and spherical cases, respectively; and γ is the adiabatic index. These equations have been normalized in terms of R_0 , the coordinate of the surface or the radius of the target; Mn_* , the critical density for light with the given wavelength; $c_{sa} = (\gamma T_0 / M)^{1/2}$, the sound velocity; and T_0 the temperature at the critical point. At the vacuum boundary the pressure is zero: $p = 0$. The boundary conditions at the source, whose coordinate $r = R_0$ is assumed to remain constant, are written in the form

$$n = n_*, \quad T = T_0 f(t), \quad u = (T/T_0)^{1/2} \quad (2)$$

and corresponds to outflow from a Chapman-Jouguet point. After the Chapman-Jouguet point is passed, the plasma flow becomes supersonic. At this point, radiation changes the temperature and the related velocity according to conditions (2), but the density remains constant. The Chapman-Jouguet point and the point with the critical density are essentially the same in comparison with the radius at which the shell appears, ~ 10 cm, and are near the target surface.¹⁷

System (1) with boundary conditions (2) determines the mathematical formulation of the problem. The time variation of the plasma production process is taken into account through a change in the initial conditions $f(t)$. From the gas-dynamics standpoint, this problem is the decay of an arbitrary discontinuity in flow with a free vacuum boundary.

System (1) was solved numerically on an Eulerian grid by a method similar to the particle-in-cell method of Ref. 18. The algorithm underwent a battery of tests which had been used previously to develop new schemes for the equations of gas dynamics.¹⁹ The ability of the scheme to reflect the specific features of the problem of the expansion of a gas into vacuum was checked through a comparison with completely conservative schemes.²⁰ In order to keep the number of grid points in the shell itself from falling below 100, we chose a total number of points $\lesssim 2 \cdot 10^3$. The step of the time integration was usually $\tau_0 = 0.2 \tau_*$, where τ_* is the extreme value permitted by the stability condition for this method. The fronts of the shock waves were smeared over up to eight zones by an artificial viscosity, but with such a fine grid this had no substantial effect on the results of the calculations.

If we take the function $f(t)$ to be a step function

$$f(t) = \begin{cases} 1, & t < \tau, \\ T_i / T_0, & t \geq \tau, \end{cases}$$

the solution of the problem in the case of a constant γ depends on $Q = T_i / T_0$, τ and the geometric factor v . The mass and energy of the plasma which is expanding in space are related unambiguously to the time τ up to the instant at which the conditions at the source change. The dynamics of the perturbation at the outflow point which is formed in the process does not depend on the time τ before it arrives at the vacuum boundary. The parameter τ thus affects the evolution of a perturbation in a comparatively late stage of the

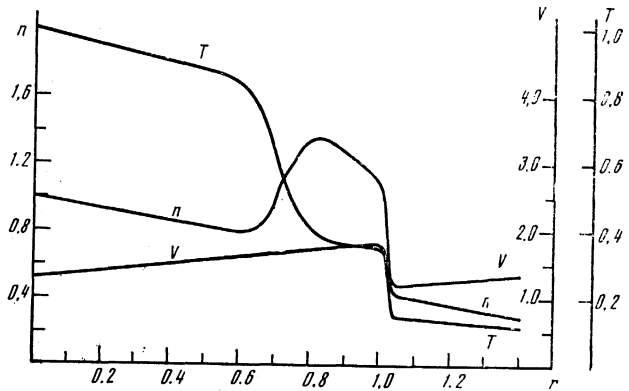


FIG. 5. Calculated profiles of (1) the density, (2) the velocity, and (3) the temperature of the plasma with distance from the target in plane geometry ($t = 1.5$).

expansion. A change in Q involves the appearance of a rarefaction region for $Q < 1$ or a compression region for $Q > 1$. Figures 5–7 show results calculated in plane geometry, cylindrical geometry, and spherical geometry with $\tau = 1$, $Q = 4$, and $\gamma = 5/3$.

As was shown in Ref. 21, the decay of the initial discontinuity of problem (1), (2) proceeds through the formation of either a pair of shock waves or a shock wave and a rarefaction wave. In plane geometry, in which the directed velocity is on the order of the local sound velocity, we are dealing with the latter of these (Fig. 5). A shock wave at $r \approx 1$ moves through the plasma of the first flow. At this shock wave, there is a jump in the temperature and also in the velocity. The second rapid increase in the temperature corresponds to the contact surface between the first and second flows. The velocity is continuous at this boundary, while the density jumps. The amplitude of this jump is determined by the pressure continuity condition, and for the given outflow conditions, (2), with a constant density at the boundary, it cannot exceed $(\gamma + 1) / (\gamma - 1)$. The slow variation in the temperature, the density, and the velocity as a function of position near the source, accompanied by a subsequent decrease in the gradients of these properties, is a consequence of the attainment of a steady-state outflow solution. The solution differs from the familiar problem of the decay of an arbitrary discontinuity in that there is a vacuum boundary. As a re-

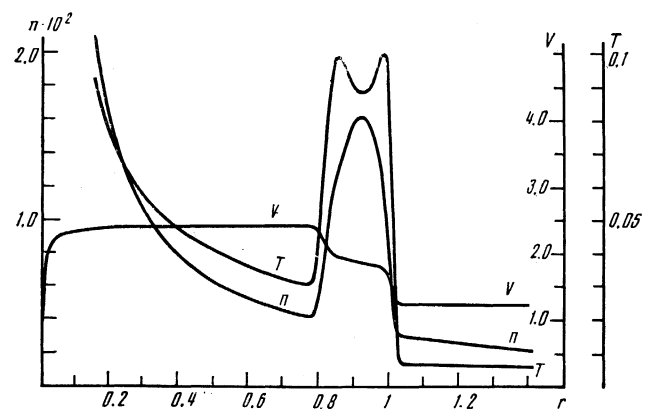


FIG. 6. Calculated profiles corresponding to Fig. 5 but for cylindrical geometry ($t = 1.5$).

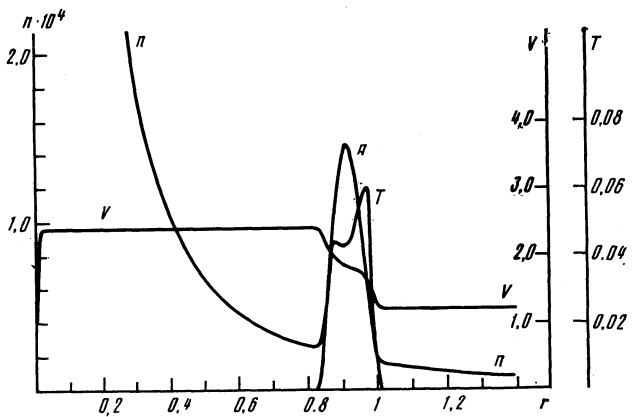


FIG. 7. Calculated profiles corresponding to Fig. 5 but for spherical geometry ($t = 1.5$).

sult, the vacuum front is accelerated. This acceleration leads in turn to a redistribution of the density, with a density maximum forming near the contact surface.

In the cylindrical case with $v = 1$, $\tau = 1$, and $Q = 4$, shown in Fig. 6, the decay of the discontinuity occurs through the formation of a pair of shock waves, which propagate away from the contact surface. One of these waves (the outer one) propagates in the first flow in the direction of the vacuum; the second (inner) wave propagates in the second flow toward the source. These shock waves are carried in the direction of the free boundary by the flow of matter, so the velocity of the inner shock wave is positive in the laboratory coordinate system. The positions of the shock wave in Fig. 6 are determined from the temperature maxima, which coincide with the discontinuities on the velocity plot. At these points, the Rankine-Hugoniot relations hold very accurately. The temperature decreases between the shock waves, reaching a local minimum roughly at the contact surface, while the density behind the shock wave continues to grow, so it reaches its maximum value in the perturbation at the same point. The ratio of the density at the maximum to that ahead of the front of the outer shock wave is greater than the limiting value of the compression attainable at the shock front, $(\gamma + 1)/(\gamma - 1)$. The thermal energy in the layer of compressed matter is an order of magnitude lower than its kinetic energy, so the layer is stable during an expansion out to large distances.

In spherical geometry (Fig. 7), in contrast to the cylindrical case, the temperature of the flows in the interaction region is even lower. Between the shock waves there is a layer of matter which has been compressed and heated by the shock waves; this layer is made up of equal numbers of particles from the first and second flows. This circumstance means that the mass fluxes across the shock fronts are equal in magnitude. The ratio of the thermal energy to the kinetic energy in the layer continuously decreases as the layer moves, reaching a value ~ 0.025 by the time corresponding to Fig. 7. This decrease is a consequence of the work performed by the inner layers of the medium on the outer layers in the course of the expansion of the matter. The compression of the medium in the layer, $\Delta = \rho_{\max}/\rho_0$ (the ratio of the density at the maximum to that ahead of the inner shock wave), increases as the layer moves toward the outer boundary. It exhibits a tendency toward limited growth when the

initial temperature increases in the region $Q \gtrsim 10$ for a given coordinate. The maximum compression Δ found in the calculations is $\Delta \approx 16 \gg (\gamma + 1)/(\gamma - 1)$. Saturation is reached primarily because of the growth of the velocity of the outer shock wave and thus the predominant unidirectional expansion of the layer toward the vacuum boundary. The high velocity of the outer shock wave determines the asymmetry which arises in the density jump, with a gently sloping front and a steeper trailing edge. This density distribution persists even after the outer shock wave reaches the vacuum boundary and the first flow is compressed. From this point on, the masses of the first and second flows in the shell are no longer equal, and the envelope itself asymptotically undergoes a further acceleration to the velocity of the second flow. In this stage, the expansion of the shell becomes inertial, with a self-similar spreading after the formation, $\Delta r/r \sim 0.1$.

Figure 8 shows density distributions of the laser plasma found experimentally, along with calculated results for a spherical target, for conditions similar to the experimental conditions, with $T \propto q^k$, where $k = 4/9$ (Ref. 11):

$$f(t) = \begin{cases} (T_1 - T_0)(t/\tau_0)^k + T_0, & t \leq \tau_0 = 0.4 \mu s, \\ T_1, & \tau_0 \leq t \leq \tau_1 = 0.6 \mu s, \\ (T_1 - T_0)[(\tau_2 - t)/(\tau_2 - \tau_1)]^k + T_0, & \tau_1 \leq t \leq \tau_2 = 1 \mu s, \\ \frac{\partial T}{\partial r} = \frac{\partial n}{\partial r} = u = 0, & T_1/T_0 = 100, \quad t > \tau_2. \end{cases}$$

Comparison of the calculated and experimental curves reveals that the results agree qualitatively and that numerical model (1) can be used to explain the formation of an envelope. The shell contains 40% of the total number of particles and 48% of the total energy out to the coordinate $r \approx 15.5$ cm. In the case of the plane target, three-dimensional effects play an important role at large length scales, and it would be incorrect to directly compare the experimental results with the numerical model (1), which predicts that there will be no compression of ions.

4. DISCUSSION OF RESULTS

It follows from these experimental and calculated results that the formation of a stable shell with a density increase $n_{\max}/n_0 > (\gamma + 1)/(\gamma - 1)$ during the expansion can be attributed to a cooling of the matter in the course of the motion. The mechanism for the cooling and the compression is clear from an analysis of the plasma dynamics in various geometric cases of the motion.

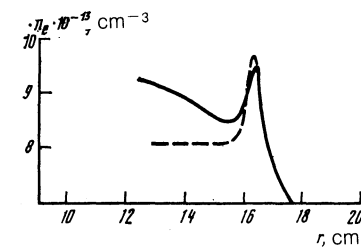


FIG. 8. Experimental (solid line) and calculated (dashed line) profiles of the density along the spatial coordinate as the shell moves ≈ 16.5 cm away from the target. The initial density in the calculation was $n'_* = 0.8 \cdot 10^{19} \text{ cm}^{-3}$.

As was shown above, in the plane case the temperature and the sound velocity vary slowly over distance near the target. Consequently, the flows collide at values $M_s \sim 1$, close to their initial values, and no gas-dynamics flow with two shock waves arises during the decay of the discontinuity. In principle, a pair of shock waves can form in this geometry and propagate away from each other; they appear in the collision of supersonic flows of matter.²¹ In this case, however, the layer of medium which lies between the shock waves and which is characterized by the parameters of these waves can undergo a change in volume only along the direction of the velocity. Accordingly, the compression of the plasma between the shock does not exceed $(\gamma + 1)/(\gamma - 1)$ as the medium moves toward the vacuum, and the thermal energy of the layer is extended on an expansion of the layer in the direction in which the shock waves are propagating.

In the cylindrical and spherical versions, the medium of the layer can cool off adiabatically, expanding in a direction perpendicular to the direction of motion. In this case the thermal energy of the plasma between the shock waves is expended on an acceleration of this plasma. The density jump at the shock fronts tends toward $(\gamma + 1)/(\gamma - 1)$ (as $M_s \rightarrow \infty$), since the shock waves are propagating through the medium near the target which has cooled off.

The plasma temperature in the layer is determined by the heating of this plasma at the shock fronts and by adiabatic cooling. The temperature accordingly decreases with distance from the wavefront, reaching a minimum near the contact surface. Taking into account the pressure equalization in the space between the shock fronts, we conclude that a density maximum $n_{\max}/n_0 > (\gamma + 1)/(\gamma - 1)$ forms at the contact surface.

In analyzing the dynamics of the shell we must note that the inner and outer shock waves move through a medium with a density which decreases continuously (basically in accordance with $n \propto t^{-\nu}$, where $\nu = 2$) during the expansion of the plasma cloud, and the velocity of these waves with respect to the medium decreases.²²

The presence of a sink for the thermal energy (a conversion into kinetic energy of the directed motion), the additional cooling due to the transverse expansion, and the decrease in the velocity of the shock waves have the consequence that there is only a slight spreading of the layer which is formed in the spherical and cylindrical cases. This result in turn has the consequence that there is an effective concentration of a large number of particles and a large amount of energy in the stable shell which detaches from the source.

CONCLUSION

The present experiments have shown that a regime of plasma expansion into vacuum in which a shell forms prevails when a target is exposed to microsecond-range, long-wave light from a CO₂ laser with a smooth pulse shape, in which case the rise time of the pulse is greater than the ion acceleration time, and the power density (10^8 – 10^{10} W/cm²) determines an approximately collisional flow of plasma with adiabatic cooling. The time variation of the energy absorp-

tion, the geometric factor, and (in particular) the type of target, which can determine the initial stage of the expansion and cooling of the plasma, play a decisive role in the formation of a stable shell with a large number of particles and with a large fraction of the initial energy at significant distances from the target. We have determined the mechanism for the formation of a cloud of laser plasma in the form of a plasma shell with a slight density increase and a large ratio $(\gamma + 1)/(\gamma - 1)$. We should also note that the processes studied here do not depend on the nature of the source, being determined exclusively by the working regime of the source. For this reason, the results found here can be used to explain, for example, the dynamics of the detachment of matter and its compression into a thin envelope during supernova explosions.²³

¹Yu. V. Afanas'ev, N. G. Basov, O. I. Kroklin et al., *Interaction of Intense Laser Beams with Plasmas* [in Russian], Scientific Progress, Radio Engineering Series, Vol. 17, VINITI, 1978, p. 5.

²A. A. Vedenov and G. G. Gladush, *Physical Processes in the Processing of Materials* [in Russian], Energoatomizdat, Moscow, 1985.

³Yu. P. Zakharov, A. G. Ponomarenko, A. M. Orishich, et al., in *Plasma Astrophysics*, International School and Workshop, Sukhumi, 1986, p. 37.

⁴A. V. Gurevich and A. P. Meshcherkin, *Fiz. Plazmy* **9**, 955 (1983) [Sov. J. Plasma Phys. **9**, 556 (1983)].

⁵V. M. Antonov, Yu. P. Zakharov, V. V. Maksimov et al., in *High-Power CO₂ Lasers for Plasma Experiments and Technology* [in Russian], Izd. ITPM, SO Akad. Nauk SSSR, Novosibirsk, 1986, p. 77.

⁶A. M. Orishich, A. G. Ponomarenko, and V. N. Snytnikov, in *Proceedings of the International Conference on Plasma Physics*, Kiev, 1987, Vol. 4, P. 173.

⁷V. M. Antonov, V. P. Bashurin, A. I. Golubev et al., *Dokl. Akad. Nauk SSSR* **289**, 72 (1986) [Sov. Phys. Dokl. **31**, 549 (1986)].

⁸Yu. P. Zakharov, in *High Power CO₂ Lasers for Plasma Experiments and Technology* [in Russian], Izd. ITPM, SO Akad. Nauk SSSR, Novosibirsk, 1986, p. 125.

⁹V. M. Antonov, in: *Higher Power CO₂ Lasers for Plasma Experiments and Technology* [in Russian], Izd. ITPM SO Akad. Nauk SSSR, Novosibirsk, 1986, p. 117.

¹⁰V. M. Antonov, Yu. P. Zakharov, V. V. Maksimov et al., Preprint 13-84, Institute of Theoretical and Applied Mechanics, Siberian Branch, Academy of Sciences of the USSR, Novosibirsk, 1984.

¹¹Yu. A. Bykovskii and V. I. Nevolin, *Laser Mass Spectroscopy* [in Russian], Energoatomizdat, Moscow, 1985.

¹²Yu. A. Bykovskii and S. M. Sil'nov, Preprint 008-87, Moscow Engineering-Physics Institute, Moscow, 1987.

¹³Yu. A. Bykovskii and S. M. Sil'nov, preprint 004-86, Moscow, Engineering-Physics Institute, Moscow, 1986.

¹⁴V. M. Antonov, V. P. Bashurin, A. I. Golubev et al., *Zh. Prikl. Mekh. Tekh. Fiz.*, No. 6, 3 (1985).

¹⁵S. V. Latyshev, Preprint 54, Institute of Theoretical and Experimental Physics, Moscow, 1982.

¹⁶G. G. Vilenskaya and I. V. Nemchinov, *Zh. Prikl. Mekh. Tekh. Fiz.*, No. 6, 3 (1969).

¹⁷S. Yu. Gus'kov, V. V. Zverev, V. Ya. Karpov et al., in *Proceedings of the Lebedev Physics Institute* [in Russian], Vol. 170, 1986, p. 93.

¹⁸O. M. Belotserkovskii and Yu. M. Davydov, *The Method of Finite-Size Particles in Gas Dynamics* [in Russian], Nauka, Moscow, 1982.

¹⁹V. N. Snytnikov, *Zh. Vychisl. Mat. Mat. Fiz.*, No. 9, 1427 (1986).

²⁰A. A. Samarskii and Yu. P. Popov, *Difference Methods for Solving Problems in Gas Dynamics* [in Russian], Nauka, Moscow, 1980, p. 108.

²¹L. D. Landau and E. M. Lifshitz, *Fluid Mechanics* [in Russian], Pergamon, 1987) Moscow, 1986, p. 519.

²²L. I. Sedov, *Metody podobiya i razmernosti v mehanike*, Nauka, Moscow, 1981, p. 304 (*Similarity and Dimensional Methods in Mechanics*, Academic, New York, 1959).

²³V. S. Imshennik and D. K. Nadezhin, *Final Stages of the Evolution of Stars and Supernova Explosions* [in Russian], Scientific Progress. Astronomy Series, Vol. 21, VINITI, 1982, p. 63.

Translated by Dave Parsons